JOURNAL OF MATERIALS SCIENCE 12 (1977) 61–74

The formation of single-phase Si-Al-O-N ceramics

M. H. LEWIS, B. D. POWELL, P. DREW
Department of Physics, University of Warwick, Coventry, UK

R. J. LUMBY, B. NORTH, A. J. TAYLOR,
Lucas Group Research Centre, Monkspath, Solihull, West Midlands, UK

Si–Al–O–N ceramics have been prepared by hot-pressing mixtures of Si_3N_4, AlN and SiO_2 (with an addition of 1% MgO) having varying ratios of AlN/SiO_2. Microstructural analysis by transmission electron microscopy and Auger electron spectroscopy has demonstrated the progressive increase in grain-boundary silicate glass in pressings prepared from compositions with excess SiO_2 to compositions given by the formula $Si_{6-z}Al_zO_zN_{8-z}$. This formula represents the simple substitution of Al for Si atoms and O for N atoms in the hexagonal βSi_3N_4 crystal. Microstructures for this "balanced" composition are essentially single phase, consiting of non–faceted, sub-micron, β' grains with a grain-boundary segregate layer of glass-forming silicate composition, containing impurity and additive metal ions, which may be detected only by Auger spectroscopy. This microstructure is in contrast with "unbalanced" compositions which contain faceted β' grains joined by a glassy silicate phase which is easily detected by electron microscopy. Final microstructural analysis combined with observations of density and phase content with progress of hot-pressing has confirmed the important role of liquid silicate formation and a "solution-reprecipitation" mechanism for densification. The presence of a 1% MgO additive is shown to accelerate this process, forming a low melting point silicate by reaction with SiO_2, assisting the early solution of AlN and the reprecipitation of β' substituted crystals.

1. Introduction

Silicon nitride (Si_3N_4) ceramics prepared by a hot-pressing process have a combination of high strength and thermal shock resistance which makes them the prime candidate for certain structural applications up to $\sim 1400^\circ$ C.

The limit to elevated temperature strength is influenced by the presence of a glassy silicate phase at β–Si_3N_4 grain boundaries which is a residue of the ceramic densification process. Evidence for the densification mechanism and accompanying conversion of α to β–Si_3N_4 has been obtained from electron microscopy and Auger electron spectroscopy [1, 2]. The mechanism is that of solution (of α) and reprecipitation (as β) with a silicate liquid forming the reactive transport medium in the form of a thin layer between transforming crystals. The origin of the silicate liquid is that of reaction between an "additive" (typically MgO) and an oxidized (SiO_2) layer on α–Si_3N_4 lath-like particles which have an extremely large surface area/volume ratio. Final microstructures contain mainly faceted β–Si_3N_4 crystals with an intercrystalline glass which is the cooled residue of the liquid sintering medium. The glass is also a sink for large impurity ions, (e.g. Ca^{2+}) which further reduce its viscosity and hence the high temperature ceramic properties.

More recently, the possibility of controlling the amount and composition of the intercrystalline phase has been realized following the discovery of highly substituted β–Si_3N_4 crystals which are formed by reacting Si_3N_4 with Al_2O_3 [3, 4]. The important implication is that substitution of Al^{3+}

for Si^{4+} (as in many sliciates) requires a simultaneous substitution of O^{2-} for N^{3-}, the oxygen being partly derived from the surface layer on Si_3N_4 particles. The formation of substituted (and expanded) β–Si_3N_4 crystals (subsequently called β') by mixing together different ratios of the stoichiometric Si_3N_4 and Al_2O_3 resulted in the proposal of a general formula $Si_{6-3x/4}Al_{2x/3}O_xN_{8-x}$ for β' [3]. It is clear from this formula that silicon vacancies are an essential feature of the structure and this has initiated the ideas of enhanced sinterability and the possibility of a substituion of further atoms (e.g. Mg or Li) on vacant sites [5]. Although X-ray diffraction indicated the presence of a small quantity of second (called "X"-phase in view of its undetermined structure) this was believed to result from the excess surface SiO_2 which had not been "balanced" for example by additions of AlN to the Si_3N_4–Al_2O_3 mixture [6]. Microstructural evidence indicated a large volume fraction of extra phases [7] and subsequent work has proved that Si_3N_4–Al_2O_3 mixtures do not form single phase β' for any composition. However, this early work has provided some of the motivation for attempts to identify compositions which give rise to single phase β' ceramics which, in turn, might have improved properties. The exploratory work of Lumby *et al.* [8] has shown that by adding an increasing amount of AlN to Si_3N_4–AlN–SiO_2 mixtures (of initial compositions corresponding to the formula above) the amount of second phase ("X"-phase for large x values and O′ – a substituted Si_2N_2O – for small x values), indicated by X-ray diffractometry, is progressively decreased. Further AlN additions replace these second phases with another phase (called "T"-phase [8] and now known to be a series of phases of different compositions but structurally similar to AlN [9]). The most nearly single phase compositions coincide with a maximum in lattice parameters for β' crystals, indicating a maximum substitution of Al^{3+}.

These compositions are approximately identifiable with the general formula $Si_{6-z}Al_zO_zN_{8-z}$. This simpler formula (which for brevity will be referred to as the z formula to distinguish it from the earlier x formula) involves a structurally simpler means of accommodation since every Si atom removed is substituted by an Al atom together with simultaneous oxygen-for-nitrogen substitution.

A significant feature of ceramics prepared from compositions near to the z formula is the increased difficulty of densification. In an attempt to produce high-strength single phase "sialons" a series of hot-pressings have been made with 1% MgO additions and basic compositions extending from the x formula to the z formula, near to a substitution level represented by $z \approx 0.8$. A series of high temperature creep measurements showed a dramatic improvement in creep resistance from x compositions to z compositions. This was taken as indirect evidence for a progressive reduction in residual second phase content at β grain boundaries.

The research described in this paper was subsequently undertaken with the following aims:

(i) A confirmation of the validity of the z formula for single phase "sialons" from microstructural evidence.

(ii) A determination of the nature and distribution of residual second phase in "unbalanced" compositions from the x and z formulae using electron microscopy and Auger electron spectroscopy.

(iii) A determination of the mechanisms for evolution of the ceramic micristructure, and of the effect of an MgO addition, using X-ray evidence for the presence of different phases at intermediate stages of the hot-pressing process.

(iv) A correlation of microstructures with available high-temperature mechanical properties.

2. Experimental techniques

2.1. Specimen preparation

The series of specimens referred to above were prepared from Si_3N_4, AlN and SiO_2 powders with varying AlN content (Table I) and 1% MgO as an aid to densification. Powder mixtures were colloid-milled in an isopropyl alcohol slurry to effect par-

TABLE I Composition and creep behaviour of 101 to 121 series of samples.

Material	Composition (wt %)				Surface tensile strain (%) (20 h, 1227° C, 77 MN m^{-2})
	Si_3N_4	AlN	SiO_2	MgO	
101	85.25	7.75	6.0	1.0	0.270
103	84.75	8.25	6.0	1.0	0.236
104	84.25	8.75	6.0	1.0	0.228
105	83.75	9.25	6.0	1.0	0.153
110	83.00	10.00	6.0	1.0	0.034
109	82.25	10.75	6.0	1.0	0.033
121	81.75	11.25	6.0	1.0	0.005

ticle size reduction to $< 5\,\mu m$ and adequate dispersion. The dried, sieved powders were hot-pressed in a graphite die at 1800° C for 1 h at a pressure of $15.4\,MN\,m^{-2}$.

2.2. Electron microscopy

Electron transparent specimens were prepared from 0.2 mm thick slices cut from the bulk pressings with an annular diamond saw. These slices were further reduced in thickness by grinding on silicon carbide papers to $< 100\,\mu m$ and finally thinned to electron transparency using 5 kV argon ion beams incident on the surface at 40°. The thinned sections were coated on both surfaces with a thin carbon film (or Au if a diffraction standard was required) to avoid surface charging in the electron beam of the JEM 200 kV electron microscope.

2.3. Auger electron spectroscopy

This technique has previously been successfully used to analyse the composition of residual intergranular phases in silicon nitride [2]. Specimens were fractured in three-point bending at 1200° C to expose the predominantly intergranular fracture surface for analysis. The first specimens to be analysed were fractured in air and quenched to 20° C within a few seconds. More recently the fracture has occurred in a vacuum of $< 10^{-5}$ Torr. The Auger analysis gave comparable results for the two procedures.

The fractured specimens were placed in the Auger apparatus with the fracture surfaces normal to the axis of the hemi-cylindrical electron velocity analyser and at 84° to the primary electron beam. Before analysis, a vacuum of 2×10^{-10} Torr was obtained in the Auger apparatus after a 24 h "bake" at 250° C. Concentration profiles from the fracture surface into the bulk specimen were obtained by progressive *in situ* removal of material with 500 eV argons ions with an ion density of $1\,\mu A\,cm^{-2}$ in an argon pressure of 5×10^{-5} Torr.

TABLE II Composition of materials A and B.

Material	Composition (wt %)			
	Si_3N_4	AlN	SiO_2	MgO
A	80.2	12.4	7.4	–
B	83.0	10.0	6.0	1.0

2.4. Phase transformation and densification analysis

Two materials, referred to for convenience as A and B (compositions given in Table II) were prepared as described in Section 2.1, except that a variety of hot-pressing temperatures and times were used (given in Table III). The presence of 1% MgO in material B enables its effect on densification and reaction to be observed. The density of each pressing was measured, and X-ray diffraction performed on powder samples with a Phillips 1010 diffractometer using Cr$K\alpha$ radiation.

3. Microstructural analysis

3.1. Electron microscopy

Fig. 1 is an example of a large electron-transparent area typical of images recorded from the series of sialons studied here. The fine grained polycrystalline structure is imaged mainly via the different diffracting conditions operating for β' grains in random orientation with respect to the incident electron beam. A detailed study of microstructure within the series of specimens (101 to 121) reveals significant differences in grain morphology, grain size and residual phase content. A high proportion of β' grains in 101 specimens (representing the x formula) have a faceted morphology in which neighbouring facets enclose angles of ~ 120°. This is particularly prominent for strongly diffracting grains in which the electron beam is parallel to the

TABLE III Variation of β' lattice parameters a and c with hot-pressing conditions.

Hot-pressing conditions		Material A		Material B	
Temperature (°C)	Time (min)	a (Å)	c (Å)	a (Å)	c (Å)
1500	60	–	–	–	–
1550	60	–	–	–	–
1600	60	7.670	2.941	7.688	2.956
1650	10	7.674	2.949	7.667	2.945
1650	60	7.648	2.934	7.639	2.929
1650	300	7.643	2.932	7.636	2.927
1700	60	7.645	2.937	7.630	2.926
1770	60	7.641	2.932	7.638	2.927
1840	60	7.641	2.932	7.634	2.927

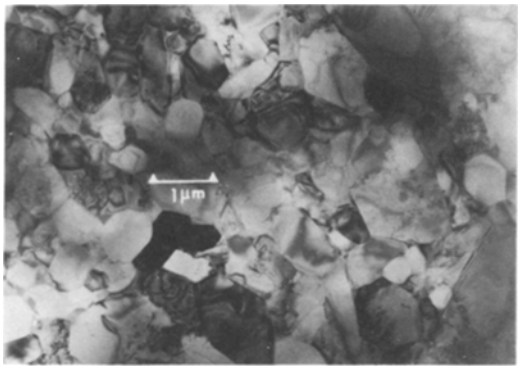

Figure 1 Low magnification transmission electron micrograph of specimen 1 0 1 in which the size of the mainly faceted grains is $\leqslant 1\ \mu m$.

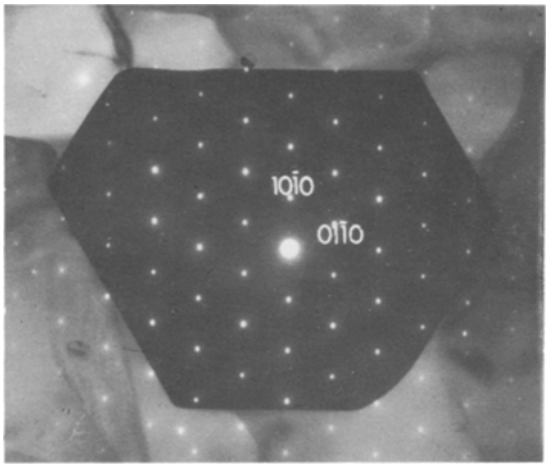

Figure 2 Transmission electron micrograph and superimposed diffraction pattern from a single faceted grain in a 1 0 1 specimen showing the hexagonal prismatic cross-section with facets parallel to $\{1\,0\,1\,0\}$ planes in the β' crystal.

that previously identified in β silicon nitride [1] and in the β' grains in $Si_3N_4-Al_2O_3$ ceramics [7]. The pronounced faceting is characteristic of crystal growth in an isotropic fluid environment, and "many beam" diffraction (Fig. 2). In Fig. 2 the inter-facet angles are exactly 120° and the facet planes parallel to $(1\,0\,\bar{1}\,0)$. Thus many of the grains have hexagonal prism shapes with occasional disturbance of some of the planar facets by impingment of neighbouring grains. Although prismatic in cross-section the grains do not have planar faces parallel to (0 0 0 1), e.g. a number of the grains in Fig. 3 have their c-axes in the image plane and thus have two sides nearly parallel to opposing facets of the prism which has rounded ends. The grain morphology is characteristic of as in the previously examined ceramics, is indicative of the presence of a liquid phase during densification. This liquid phase is retained in intercrystalline spaces during cooling from the hot-pressing temperature and forms a glass phase (marked g in Fig. 3), identifiable by its lack of diffraction contrast and susceptibility to electron irradiation damage [1].

Proceeding through the series 1 0 1 to 1 2 1 there is a progressive reduction in the amount of intercrystalline glassy phase. It is still detectable in specimen 109 at grain triple junctions and in many of the grains two neighbouring 120° faceted surfaces are still visible. On examination of the 121 specimen (representing the z formula) there is a pronounced change in grain morphology and absence of residual glassy phase. In Fig. 4 the grain boundaries have images similar to those from a metallic polycrystal, i.e. smoothly curved inter-

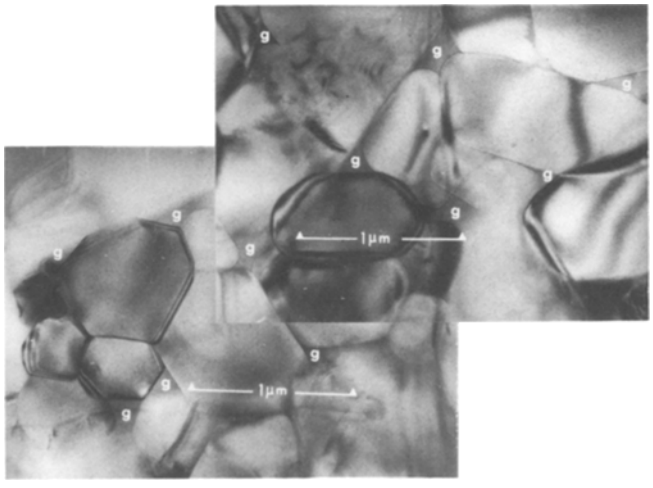

Figure 3 Transmission electron micrograph showing typical faceted grain morphology and associated inter-crystalline glassy phase (g) in specimen 1 0 1 (corresponding to an x formula composition).

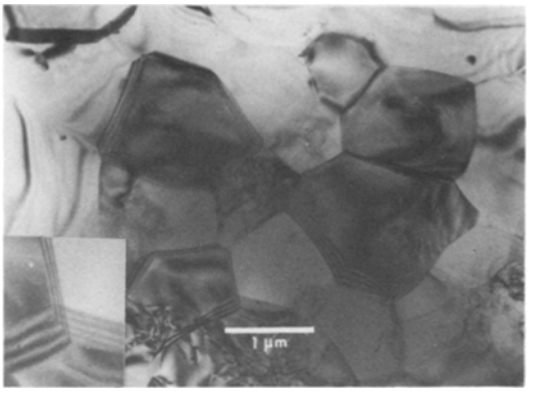

Figure 4 Transmission electron micrograph showing irregular (non-faceted) grain boundaries and absence of inter-granular glass in specimen 1 2 1 (corresponding to a z formula "balanced" composition). The inset image (at higher magnification) emphasizes the sharpness of triple junctions via the meeting of three sets of thickness extinction contours.

faces with sharp triple junctions. These features are revealed mainly by thickness extinction contours at the boundaries between differently diffracting crystals in a single phase material on solidification or recrystallization. An approximately two-fold increase in mean β' grain size occurs from specimen 1 0 1 to 1 2 1 which may be explained by the inhibiting effect of the residual grain boundary phase on grain growth. Thus grain-boundary migration involves a diffusional transfer of atoms across the boundary which for specimens 1 0 1 etc requires the solution and reprecipitation of β' components.

3.2. Auger electron spectroscopy

A comparison was made between Auger spectra from fracture surfaces of 1 0 1 and 1 2 1 specimens for different positions below the original fracture surfaces. Fig. 5 shows the change in a typical set of spectra (for Auger energies between 0 and 600 eV) taken from sialon 1 2 1 with progressive removal of material from the fracture surface. The elements Si, Ca, N and 0 are identified by Auger peaks at similar energies to those previously observed in hot pressed silicon nitride [2]. The carbon and argon peaks arise from contamination and ion-bombardment respectively and the Al peak is an addition to the spectrum expected in sialons. A Mg peak appears at higher Auger energies similar to previously published spectra for silicon nitride [2] and is not reproduced here.

Assuming that the Auger peak height in the differential spectrum is proportional to the element

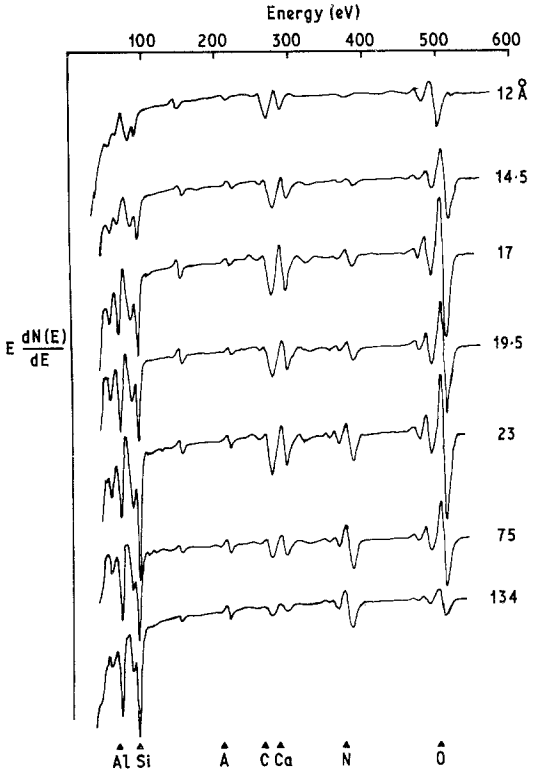

Figure 5 Typical set of Auger electron spectra (from a 1 2 1 specimen) showing the increase or decrease in different element concentrations with distance from an intergranular fracture surface. The figures against each spectrum are calculated thicknesses of material removed by sputtering.

concentration in the surface it is possible to compare the thickness of grain-boundary phases in specimens 101 and 121 and to estimate the phase constitution with reference to spectra from a standard of similar composition. The nitrogen peak is used as a reference in plotting the concentration of other elements in Fig. 6a and b. The position, in thickness of sputtered material, at which the N peak is first observed differs markedly from specimen 1 0 1 to 1 2 1 and is approximately at the positions first plotted on the concentration profiles for other elements in Fig. 6a and b. The rapid fall in O/N, Ca/N and Mg/N ratios is, therefore, partly influenced by the growth in the N peak but mainly by the decrease in O, Ca and Mg concentration. It is clear that the additive and impurity elements (Mg + Ca) are segregated to a grain-boundary oxygen-rich "phase" and that the thickness of this phase is much greater for the 1 0 1 specimen. Precise values for the thickness of the residual grain-boundary phase from Auger analysis can not be made because of a large

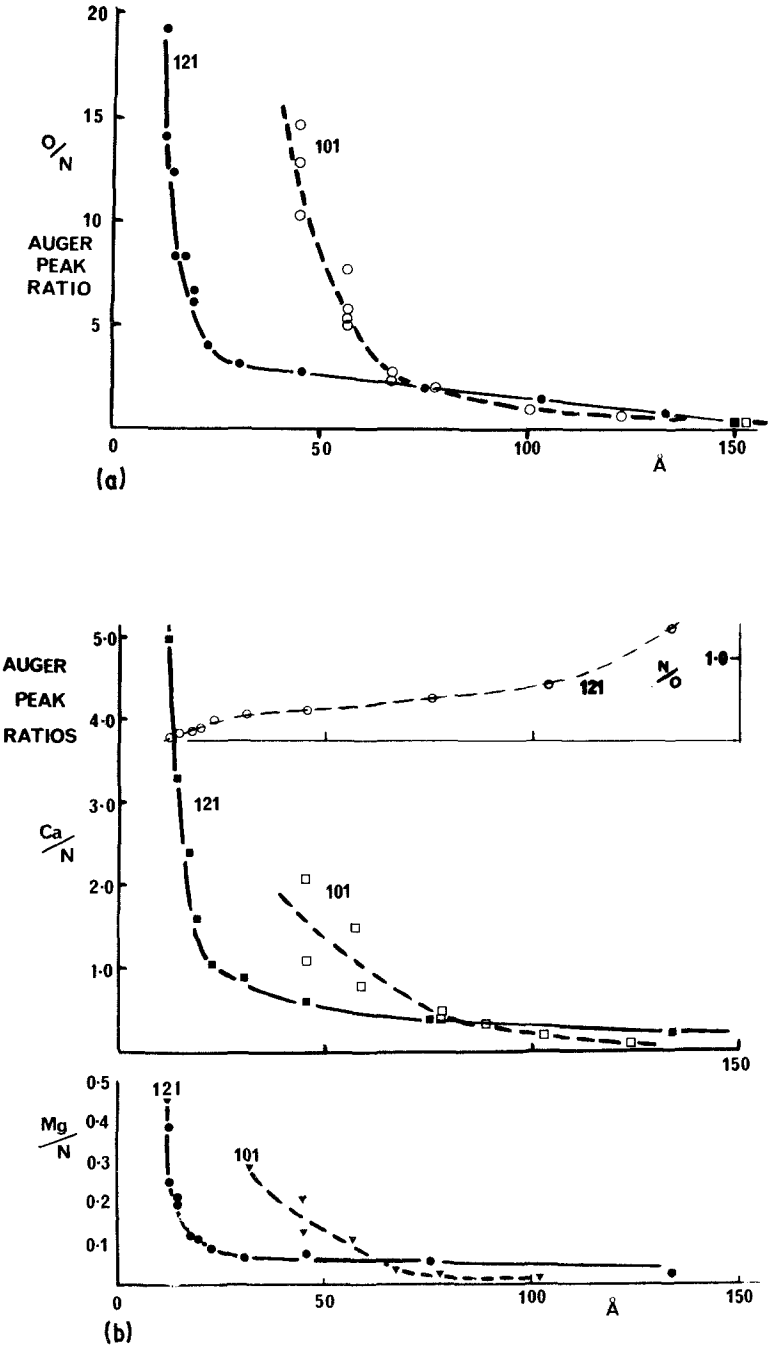

Figure 6(a) and (b) Variation in concentration of additive and impurity elements indicated by variation in Auger peak height with distance from the intergranular surface. The values are shown with reference to the nitrogen peak for the 1 0 1 and 1 2 1 specimens.

potential error in the calculated sputtering rate on which the horizontal axes in Fig. 6a and b are based. It is also evident form the images in Fig. 3 that the glassy phase in specimen 1 0 1 varies markedly in thickness, especially near β' grain triple junctions, and this is reflected in the slower reduction in Ca/N + Mg/N ratios with distance from the initial surface. There is also a "blurring" of the interfaces due to the effects of ion bombardment. The Al concentration does not show a similar rapid decrease with distance from the initial surface, consistent with the solubility of this element in β' crystals.

A qualitative analysis of the grain-boundary

TABLE IV Grain boundary AES analysis (10 Å layer average)

	CaO	MgO	Al_2O_3	SiO_2
Si_3N_4–MgO	0.4	0.75		2
SiAlON 1 0 1	0.15	0.64	0.22	2
SiAlON 1 2 1	0.076	0.42	0.22	2

phase has been made from averaged Auger data for a 10 Å thick layer following removal of surface contamination (~ 10 Å during which the oxygen peak initially increases in size). The values in Table IV have been calculated by comparison with Auger spectra from glass standards having the composition of cordierite, $2MgO$, $2Al_2O_3$ $5SiO_2$ and a previously prepared $CaO \cdot MgO \cdot 2SiO_2$ glass [2]. The values are listed as mole fractions of the component oxides with reference to SiO_2 and compared with previously determined data for hot-pressed silicon nitride with an MgO additive [2]. The relatively high SiO_2 levels indicate a phase of glass-forming composition, consistent with microscopic and diffraction observation of the 101 specimen. The analysis for the 1 2 1 specimen suggests that a similar glass-forming phase is present although this is not detected by electron microscopy. This apparent contradiction can be rationalized if the grain-boundary phase consists of an intercrystalline layer of thickness ~ 10 Å, i.e. below the limit of resolution for carbon-coated specimens even for grain boundaries which are parallel to the electron beam. The Auger profiles are consistent with this thickness especially when allowance is made for the initial contamination layer.

The relative concentration of MgO etc, in specimens 101 and 121 requires explanation in view of the significant differences in volume fraction of glassy phase. A constant amount (1 wt%) of MgO was present in all members of the series 1 0 1 to 1 2 1, hence if the solubility of MgO in β' crystals is negligible a much higher concentration is expected in the very small residual phase volume of the 1 2 1 specimen compared with the 1 0 1 specimen. The slightly lower value for the 1 2 1 specimen (0.42 compared with 0.64) suggests either that the MgO is preferentially removed from the 1 2 1 hot-pressing by vapourization (in the absence of a liquid host) or that it can be accommodated in the β' structure. The latter suggestion would be favoured from evidence given by Hendry *et al.* [5] but since this explanation of solubility is based on a vacancy-containing host β' structure the question remains unresolved. The Auger evidence from surfaces remote from original fracture favours the explanation of a small solubility of both MgO and CaO in the β' structure especially in the absence of a liquid host (compare the 1 2 1 and 1 0 1 profiles for Ca and Mg for large depths below the initial fracture surface). The presence of CaO is explained by the impurity content of Si_3N_4 in the initial mixture as in previous analyses of hot-pressed material from the same source [1]. However, the generally lower CaO concentrations in the "sialons" are difficult to rationalise in view of the comparable glass content of sialon 1 0 1 and the silicon nitride hot-pressing with 7% MgO additive [1]. In this case the argument for enhanced calcium solubility in β' crystals (compared with β Si_3N_4) is less convincing because of the larger ionic size of Ca^{2+} compared with Mg^{2+}.

For some elements, additional information concerning their chemical environment is available from Auger peak shifts (chemical shifts) and this has previously been used to distinguish Si in β Si_3N_4 crystals and that in the grain-boundary silicate glass [2]. Similar shifts in Al peak position have not been observed for Al atoms known to be in the two different chemical environments in these experiments. Hence the observed absence of shifts for Ca and Mg with progress of surface sputtering cannot be taken as evidence against their solubility in the β' crystals. Further, it is less likely that shifts in the higher energy Ca and Mg peaks would be detectable because of the reduction in instrumental resolution and deeper energy levels involved in the Auger process.

4. Phase transformations and densification during hot-pressing

Materials A and B, treated as described in Section 2.4, were examined and the results discussed below.

4.1. Densification

Fig. 7 compares the densification behaviour of materials A and B. These values were determined by preparing pressings at each individual temperature, holding for 1 h at a pressure of 15.4 $MN\,m^{-2}$. It can be seen that the presence of 1% MgO markedly enhances densification especially at lower temperatures, and allows the final density to be reached at a lower temperature.

Fig. 8 gives the results of a series of experiments in which time was varied at a hot-pressing

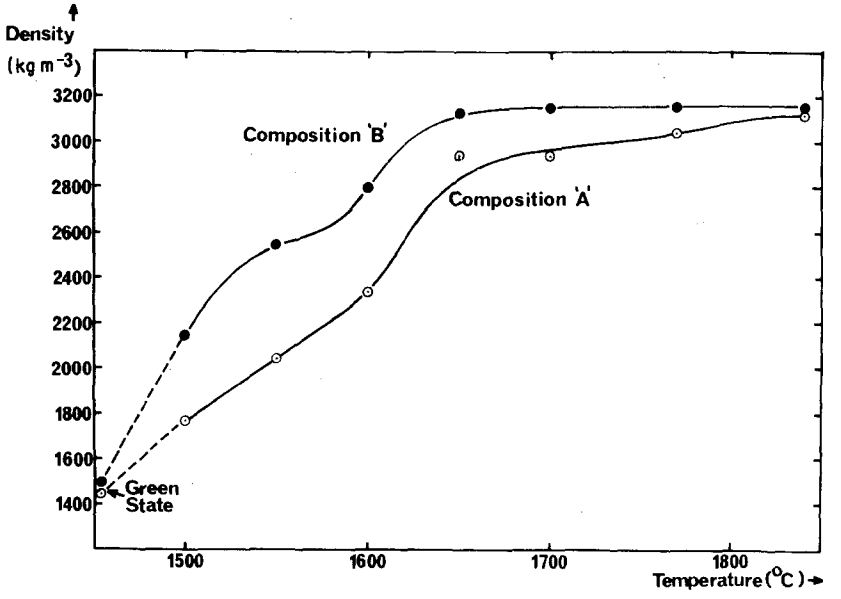

Figure 7 Variation of final density with hot-pressing temperature.

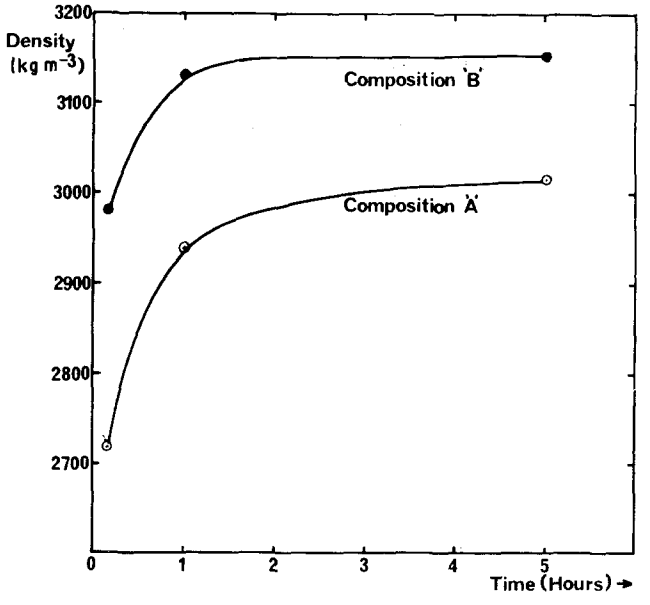

Figure 8 Variation of final density with time at 1650° C.

temperature of 1650° C. This temperature was chosen as one at which the rate of densification was high. The improved densification exhibited by material B again demonstrates the advantage of the MgO addition.

4.2. Phase transformations

The materials described above were ground up and examined by X-ray diffraction in order to identify the phases present, their proportions, and the lattice parameters of the expanded β Si_3N_4. X-ray diffraction was performed on the powder samples using a Phillips 1 0 1 0 diffractometer using Cr$K\alpha$ radiation. Approximate phase proportions were determined by comparing peak areas with those obtained from standards, whilst lattice parameters were determined from a number of peaks using a least-squares analysis.

Fig. 9a and b shows the changes in phase content which occur at hot-pressing temperatures

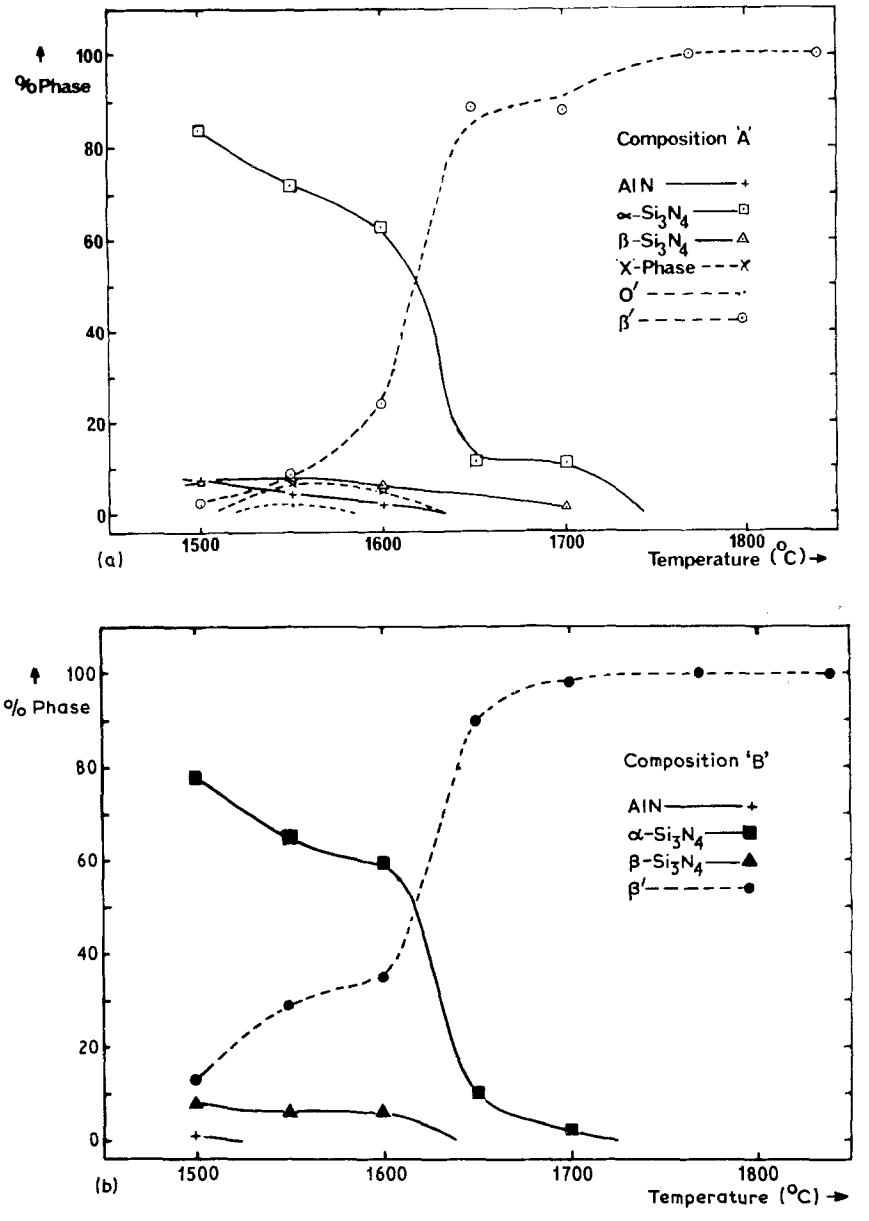

Figure 9 Variation of crystalline phase content with hot-pressing temperature (a) composition A; (b) composition B.

between 1500 and 1840° C. Fig. 10 describes the changes occurring with time at 1650° C. It can be seen that although the MgO has not significantly influenced the rate of disappearance of α- and β-Si_3N_4, it has hastened the removal of AlN and the appearance of expanded β-Si_3N_4. Other points of note are that Si_2N_2O (or O^1) and X-phase are observed in material A where MgO was absent. Fig. 10 shows that in the later stage of the reaction (after 10 min at 1650° C, all of the AlN has disappeared) the MgO does not influence the removal of α- and β-Si_3N_4.

The influence of hot-pressing time and temperature on the lattice parameters a and c of the expanded β-Si_3N_4 is given in Table IV. These results demonstrate that a highly substituted β' forms first. The MgO addition aids early β' formation giving rise to a higher degree of substitution. The slight difference in final lattice parameters between materials A and B can be explained by the small discrepancies in composition (material A in composition (material A contains more AlN and SiO_2, which produces a higher substitution level). The influence of time is similar in that as reaction

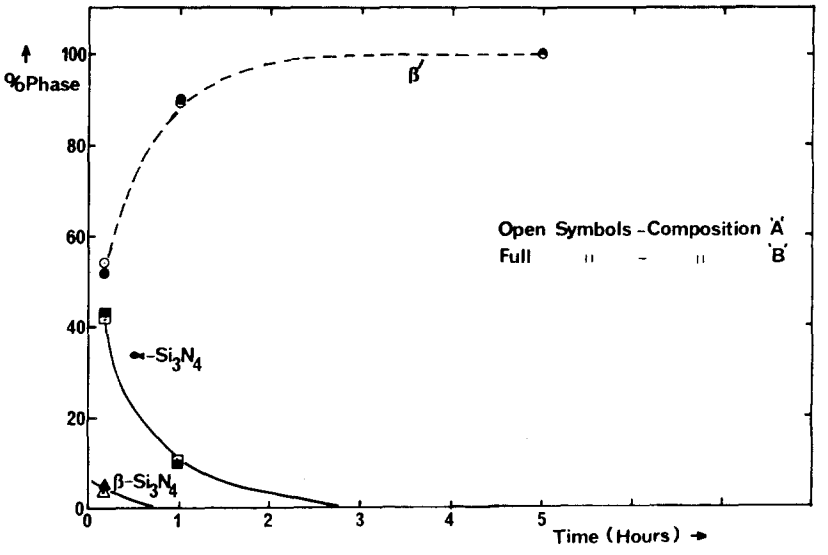

Figure 10 Variation of crystalline phase content with time at 1650° C.

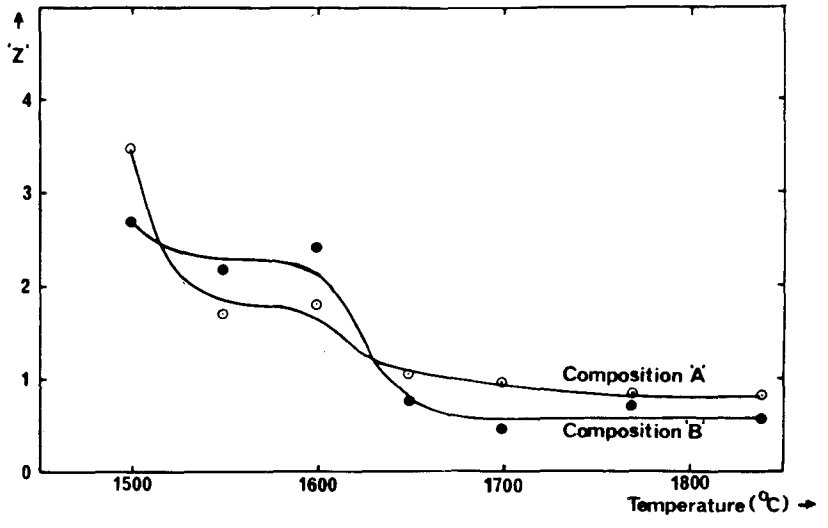

Figure 11 Variation of z with hot-pressing temperature.

proceeds a and c decrease to a minimum value.

An estimate of substitution level (z) has been obtained from the a lattice parameter. Figs. 11 and 12 show the variation of z with temperature and time. The high values of z obtained from materials hot-pressed at 1500 and 1550° C were obtained from the angle of the 1 0 1 reflection. (Insufficient β' was present below 1600° C to permit accurate determination of lattice parameters, and so these values are only approximate.) The initial high substitution values shown at 1550° C drop to a plateau at 1550 to 1600° C after which further reaction allows the z value to decrease to its limiting value.

4.3. Densification and reaction

Analysis of the density and phase relationship data together allows the following general points to be made:

(1) Most rapid densification occurs between 1550 and 1650° C, at which temperature AlN and SiO_2 have reacted completely.

(2) The more rapid densification of material B (containing MgO) is associated with the earlier dis-

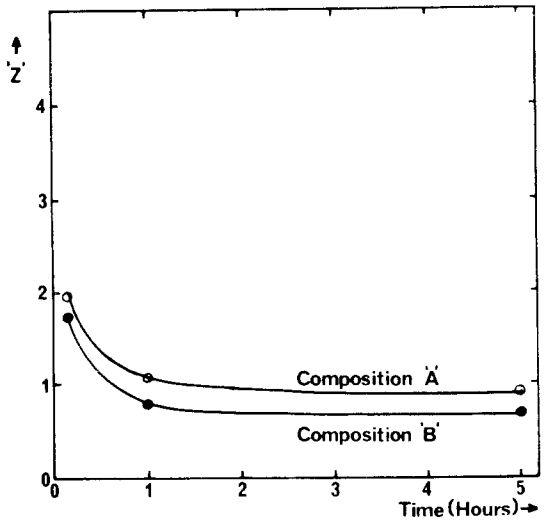

Figure 12 Variation of z with time at 1650° C.

appearance of AlN and, by inference, SiO_2. One result of this is that more β' forms earlier; another is that intermediate products such as X-phase are "by-passed" or disappear at lower temperatures. Once the AlN and SiO_2 have gone, the densification behaviour of materials A and B is similar. MgO thus improves densification associated with more rapid reaction of AlN and SiO_2.

(3) The main effect of the MgO addition is to accelerate the early densification. The higher absolute values of density associated with the presence of MgO is primarily due to its beneficial effect in the early stages of the reaction.

(4) The low temperature values for the substitution level z of the β', even with their inevitable inaccuracy, suggest that β' of even higher levels of substitution are present at the very start of its formation. The upper limit for the z value is probably 4 resulting from the reaction:

$$2SiO_2 + 4AlN \rightarrow Si_2Al_4O_4N_4.$$

5. Discussion

5.1. The densification mechanism

Analysis of microstructure by electron microscopy and Auger spectroscopy together with the X-ray and density measurements at intermediate stages of hot-pressing provide evidence for a solution and reprecipitation mechanism for densification. The importance of the MgO additive in promoting the rapid formation of a reactive silicate liquid below the hot-pressing temperature is demonstrated by the X-ray and density observations.

The densification mechanism is essentially that previously presented for hot-pressed silicon nitride ceramic [1] with a number of modifications. Broadly, it may be considered to occur by the following stages, although it must be emphasized that these stages are by no means discrete and considerable overlap will occur:

(i) Initial liquid formation (enchanced by MgO), facilitating particle re-arrangement.

(ii) Dissolution of AlN and the formation of X-phase liquid and β' with a z value of about 4 via the approximate reactions:

$$SiO_2 + AlN \longrightarrow SiAlO_2N \quad \text{(X-phase)} \quad (1)$$

$$SiO_2 + 2AlN \longrightarrow \tfrac{1}{2}(Si_2Al_4O_4N_4) \quad (z = 4\beta'). \quad (2)$$

The presence of MgO accelerates both these reactions and the accompanying densification, meaning that both finish at an earlier stage in the hot-pressing cycle. It appears that the greater reactivity of SiO_2 relative to AlN favours reaction (1) initially, but reaction (2) subsequently dominates due to the balance of constituents.

(iii) Dissolution of Si_3N_4 (both α and β) and re-precipitation as more β' whose substituion level falls as the reaction proceeds. Porosity is simultaneously removed. MgO does not appear to increase the rate of either phase transformations or densification at this stage.

The incorporation of ions from the liquid silicate phase into the β' crystals is best achieved by the use of "balanced" compositions given by the formula $Si_{6-z}Al_zO_zN_{8-z}$. For "unbalanced" compositions the excess SiO_2 must compete with β' for solution of Al and Mg resulting in the formation of a residual intergranular silicate phase.

Dense materials may be obtained by hot-pressing appropriate proportions of the basic constituents Si_3N_4, AlN, SiO_2 and Al_2O_3, an initial reaction between SiO_2 and Al_2O_3 (possibly in the from of surface layers) resulting in silicate liquid formation at $\sim 1600°$ C facilitating densification and reaction. However, it is often advantageous to add small amounts of metal oxides such as MgO, thus causing silicate liquid to form at a lower temperature. The lower viscosity of this liquid speeds up densification and reaction in the early stages at least.

However, in attempts to achieve ease of densification together with low residual phase content

the question of solubility of the additive in the β' structure must be considered. The accommodation of, for example, Mg in constitutionally vacant β' sites is not applicable to the revised formula $Si_{6-z}Al_zO_zN_{8-z}$. Other possibilities are: (i) the direct substitution of Mg for Si and Al, and (ii) the accommodation of Mg on intersititial sites associated with $Al(ON)_4$ tetrahedra in the β' structure. These two cases give rise to general formulae for the five-element compounds:

(i) $Si_{(6-z-2i)}Mg_iAl_{(z+2i)}O_zN_{8-z}$ and

(ii) $Si_{(6-z+s)}Mg_sAl_{(z-2s)}O_zN_{8-z}$, and

where s and i refer to the number of Mg atoms per unit cell of β'. Neither formula is satisfied by the simple addition of MgO to compositions given by the z formula (e.g. (i) requires additions of Mg_2SiO_4 and/or $MgAl_2O_4$). Current research is directed towards an identification of optimum compositions which will enable single-phase materials with desired properties to be produced, even with increased additive contents.

The need to explore the solubility of a fifth element stems partly from the relatively high melting point and viscosity of silicates formed with Al. The solubility of elements other than Mg (for example, the transition metals) requires further investigation since many of these elements give rise to low viscosity silicates and some might be capable of incorporation into β'.

5.2. Mechanical properties

A previous survey of high-temperature creep properties for the series of sialons (1 0 1 to 1 2 1) has demonstrated the marked increase in creep resistance as the "balanced" composition (z-formula) is approached. These results were used as indirect evidence for a progressive decrease in the amount of grain-boundary phase from x to z compositions, the inference being that the creep strain arises from grain-boundary sliding, possibly by viscous flow in a glassy phase. This hypothesis is confirmed by the direct microstructural observations presented here and by the absence of slip-dislocations in creep-specimens. A simplified model for this deformation process is presented in Fig. 13 which shows a number of interlocking non-deformable grains of hexagonal cross-section linked by an intergranular viscous phase above the glass transition temperature. The grain-boundary

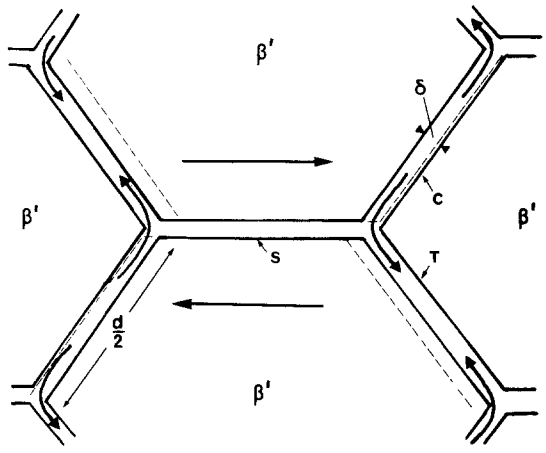

Figure 13 Simple model for creep deformation via grain-boundary viscous flow. The rate-controlling process of flow from compressive (C) to tensile (T) facets is indicated by curved arrows. The mechanism will not result in steady state creep because δ (the mean thickness of viscous phase associated with compressive facets) decreases with time.

shear (indicated by straight arrows across boundary S in Fig. 13) will develop alternate tensile and compressive stress components normal to grain-boundary facets T and C. It is probable that the creep-rate will be controlled by the transport of matter from compressive to tensile facets (indicated by the curved arrows in Fig. 13). In this respect the sliding model is similar to that described by Gifkins [10] with reference to single-phase metals. The essential difference between the two cases is concerned with the nature of the grain-boundary. For the single-phase metal, transport of matter is via diffusion along grain boundaries which maintain an approximately constant structure and are simply displaced from their initial position. For the ceramic model the crystal grains (of β') are displaced by the viscous flow of non-crystalline phase between C and T boundaries in which the phase thickness δ changes with strain. Creep deformation for the single-phase model is described by a steady-state strain rate $\dot{\epsilon}$ which is proportional to the grain-boundary diffusion coefficient. In contrast the ceramic model predicts a non-steady-state process because $\mathring{\epsilon}$ will be controlled by the viscous flow of grain-boundary phase enclosed by the compressive facets C which exhibit a decrease in separation, δ, with strain. A simple analysis (see e.g. [11]) of viscous flow between two plates under constant normal stress surrounded by a reservoir of fluid indicates that

the velocity of separation $d\delta/dt$ varies as δ^3. Thus to a first approximation the creep curve will have the form $\epsilon_{(\tau,T)} \approx (1/d)[\delta_0 - (K/\sqrt{t})]$ in which the constant K is a function of η, the grain-boundary phase viscosity, τ, the applied shear stress, and d, the grain size. δ_0 is the initial grain-boundary phase thickness. Quantitative comparison with experimental data is not appropriate in view of the idealized nature of the model but qualitative features of creep curves for the 1 0 1 to 1 2 1 series of sialons are in agreement with the predictions of (i) a progressively decreasing value of $\dot{\epsilon}$, and (ii) a rapid decrease in $\dot{\epsilon}$ for those specimens characterized by smaller grain-boundary phase thickness δ_0. The approach to zero creep-rate (when δ for compressive facets approaches zero thickness) will normally be interrupted by the nucleation of cavities in the viscous phase associated with tensile facets and the expansion of these cavities by viscous flow round them, resulting in fracture. The limiting strain (ϵ) at which zero-creep rate is approached is given approximately by $\epsilon \simeq \delta_0/d$. Using approximate values of $d = 1\,\mu m$ and $\delta_0 = 100$ and 10 Å (for specimens 1 0 1 and 1 2 1 respectively) the calculated values of $\epsilon =$ 0.1% and 0.01% are in reasonable agreement with observed creep strain levels [8] for 1 0 1 and 1 2 1 specimens after 20 h at 1227° C and 77 MN m^{-2} (0.27% and 0.006% when the creep curves have nearly zero slope).

An alternative creep machanism for ceramics containing residual glassy intergranular phases is that of dissolution (e.g. of β') of grains at compressive facets and reprecipitation on tensile facets. This is a steady-state process with the grain-boundary phase (of constant thickness) forming the channel for rapid diffusion. This mechanism is unlikely to be rate controlling except for extremely small values of δ_0 or following creep by the viscous flow mechanism when δ has been reduced to a small thickness. The creep mechanism is then comparable with that for a single-phase polycrystal described above.

A different creep mechanism has been suggested by Kossowsky *et al.* [12], based on experimental observations of tensile creep on two grades of silicon nitride (HS110 and HS130). They have observed the characteristic three-stage creep curve and identify primary creep with cavity nucleation in the viscous phase at triple junctions followed by steady-state creep during which the cavities spread across grain facets and finally link-up to propagate as large cracks during tertiary creep, prior to intergranular failure. The model is supported by experimental evidence for cavitation, together with an activation energy for steady-state creep appropriate for viscous flow in silicate glasses. However, the model does not predict the shape of the creep curve; there is no obvious reason why cavity growth should result in steady-state creep and there is no clear distinction between the three-stages of crack growth. They have related the observed times to failure (t) with the steady-state creep rate $\dot{\epsilon}$ using the expression:

$$t = \frac{1}{\dot{\epsilon}} \left[\frac{8\pi l (1-\nu)\gamma}{\mu d^2} \right]^{\frac{1}{2}}$$

where l is the grain facet size, γ the effective fracture surface energy, and μ the shear modulus. However, this prediction is based on a model for cleavage nucleated by crystal plasticity [13] and is not applicable to a creep failure based on cavity growth by viscous flow.

The improvement in high-temperature creep and delayed fracture properties for "sialon" type ceramics may be achieved either by reducing the amount of residual phase towards "balanced" compositions similar to the 1 2 1 specimen studied here or by adjustment of its composition to increase viscosity or to induce crystallization. Increased viscosity in the residual phase may reflect an undesirable increase in liquid-phase viscosity during processing, resulting in more difficult densification. The best compromise between ease of processing and good high-temperature properties is likely to be achieved with an additive (or additives) which promote crystallization of the residual phase, thus eliminating the more rapid viscous flow mechanisms for creep and delayed fracture.

Acknowledgements

The authors wish to thank the Directors of Lucas Industries Limited for permission to publish this paper. In addition the help of Mr R.E. James and Miss K.H. Ednie with the X-ray diffraction work is gratefully acknowledged.

References

1. P. DREW and M. H. LEWIS, *J. Mater. Sci.* 9 (1974) 261.
2. B. D. POWELL and P. DREW, *ibid* 9 (1974) 1867.
3. K. H. JACK and W. I. WILSON, *Nature* 238 (1972) 80, 28.

4. Y. OYAMA and O. KAMIGAITO, *Jap. J. Appl. Phys.* **10** (1971) 1637.
5. A. HENDRY, D. S. PERERA, D. P. THOMPSON and K. H. JACK, "Special Ceramics 6", edited by P. Popper (British Ceramic Research Association, Stoke-on-Trent, 1974) pp. 321–31.
6. Lucas Industries Patent, German Patent Publication 2354024, March 1974.
7. P. DREW and M. H. LEWIS, *J. Mater. Sci.* **9** (1974) 1833.
8. R. J. LUMBY, B. NORTH and A. J. TAYLOR, in [5] pp. 283–98.
9. K. H. JACK, *J. Mater. Sci.* **11** (1976) 1135.
10. R. C. GIFKINS, *J. Inst. Met.* **95** (1967) 373.
11. A. H. COTTRELL, "The Mechanical Properties of Matter" (Wiley, 1964) p. 223.
12. R. KOSSOWSKY, D. G. MILLER, and E. S. DIAZ, *J. Mater. Sci.* **10** (1975) 983.
13. J. A. WILLIAMS, *Phil. Mag.* **20** (1969) 635.

Received 13 April and accepted 4 May 1976.